The IRM Quarterly
Fall 2003, Vol. 13, No. 3

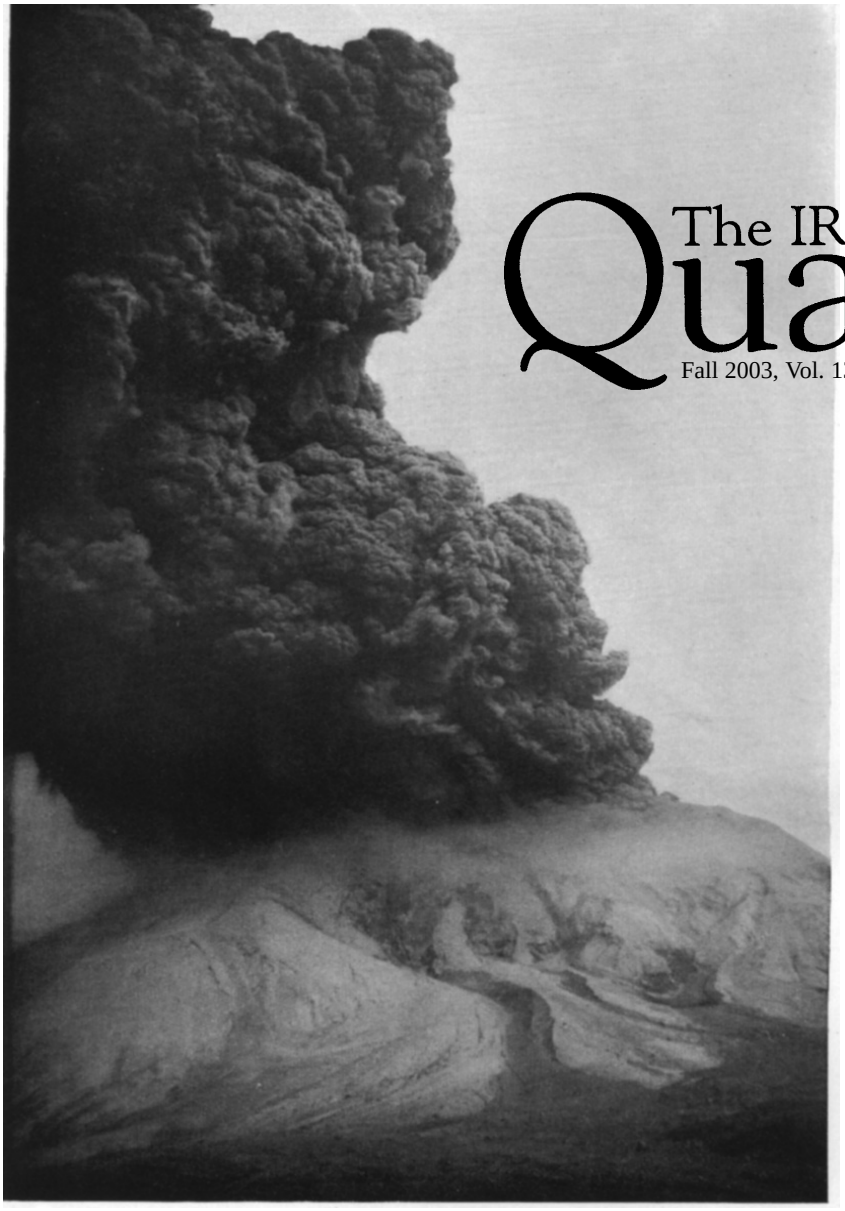

Clouds of gas and ash rise from Vesuvius, April 1906

From ***The Vesuvius Eruption of 1906: Study of a Volcanic Cycle****, by Frank A. Perret, Carnegie Intitute of Washington, 1924*

Maintaining Standards III
Pozzolana Cement
cross-calibration samples available

Mike Jackson
IRM
Leonardo Sagnotti
Istituto Nazionale di Geofisica e Vulcanologia (INGV)
Pierre Rochette
Centre Européen de Recherche et d'Enseignement des Géosciences de l'Environnement (CEREGE)
Peter Sølheid
IRM

Last year we carried out an interlaboratory cross-calibration exercise that involved the 10 labs of the MAGNET consortium, as well as the Bremen and IRM labs [*Sagnotti et al*., 2003; see also *MAG-azine n.3 and 4*]. Measurements involved low-field susceptibility, anhysteretic remanence (magnetized at INGV), and anhysteretic susceptibility (i.e., new ARMs magnetized in the other labs). One of the materials we used as a standard of comparison was a commercial Italian cement "pozzolanico," and whereas we found very good interlab consistency in susceptibility and remanent moment determinations, there was a suprisingly large variation in reported values of anhysteretic susceptibility. We are now making samples of this material available for wider distribution and additional interlaboratory standardization.

The Eternal Cement

Even before we get to its magnetic properties, this is rather interesting material. The name *pozzolana* (a.k.a. *pozzuolana*) is derived from the Latin *pulvis puteolanus* (powder from Puteoli, now Pozzuoli, a historical town on the northwestern side of the Golfo di Napoli) and refers to unconsolidated pyroclastic deposits erupted by the Campi Flegrei volcanic field during the Pleistocene and the Holocene. In ancient times (~3rd Century BCE) it was discovered that mixing these pozzolanic deposits with lime produced an exceptional cement. Vitruvius, in his ten-volume *De Architectura*, devotes a chapter (Book II, ch. VI) to this "powder which, by nature, produces wonderful results. It is found in the region of Baia and in the lands of the municipalities round Mount Vesuvius. This being mixed with lime and rubble, not only furnishes strength to other buildings, but also, when piers are built in the sea, they set underwater." It was one of the first examples of what is called a "hydraulic cement." The harbor works at Puteoli were constructed *ca* 199 BCE with pozzolana cement.

Pozzolanic materials by themselves are not cements, but they contain silica (and alumina) in a reactive form. The pozzolana cements of classical antiquity were made simply by mixing volcanic pozzolana with lime (CaO, produced by heating limestone). As additives in modern portland cements, pozzolans improve mechanical strength and provide resistance to physical and chemical weathering. Natural pozzolans are not restricted to the ash deposits of Campi Flegrei and Vesuvius. Three distinct pozzolana units are now formally defined in the sequence of volcanic products erupted by the Alban Hills, upon which the town of Rome was (and still is) founded. In commercial building materials the name is now widely applied to volcanic components of suitable composition, regardless of their source. Artificial pozzolans are also used in modern commercial cements; these are derived from fly ash, produced by coal-burning power plants, incineration of municipal solid waste, etc.

In modern portland cement the chief raw materials are limestone, chalk, etc. (which supply lime), and clays or shales (which provide alumina (Al_2O_3) and

pozzolana

continued on p. 8...

Low-temperature, high-temperature, and hysteresis properties of sediments from White Lake, northwestern New Jersey

Yongxiang Li
Lehigh University
yol5@lehigh.edu

Since millennial to decadal climatic oscillations were recognized as fundamental features of our climate system, there has been growing interest in employing multiproxies to reconstruct climate change during the Quaternary. The magnetic variation of lake sediments, used as an independent climatic proxy, is often attributed to the changes in climatically-driven detrital input into a lake. The magnetic mineral - climate link in organic-rich sediments, however, has not been extensively investigated. As part of ongoing interdisciplinary work, a magnetic study was conducted on sediments from White Lake (41.0°N, 74.8°W), northwestern New Jersey, to examine whether the magnetic properties of White Lake sediments recorded climate change. Low-temperature (LT), high-temperature (HT), and hysteresis measurements of selected samples from a core taken from the deepest part of the lake were carried out at the IRM to characterize the magnetic minerals, the carrier of possible magnetic-climatic signatures, in lake sediments. The core recovers a ~ 14,000 year record and contains a succession from pale grey clay-rich sediments, through light brownish marl (calcium carbonate precipitated by aquatic plants), to dark gyttja (organic-rich mud). Each of these three compositional components exhibit different magnetic properties.

The clay-rich sediments occur at the base of the core and are characterized by strong magnetization and pronounced LT phase transitions. The LT experiments show a sharp decrease in SIRM at ~120 K (Figure 1a), indicative of magnetite (Verwey, 1939). The rapid drop in LTSIRM while warming through ~35 K and the lack of changes in the RTSIRM during cooling at ~35 K (Figure 1a) suggest that some phases such as siderite, ferrihydrite, and ilmenite probably reside in the clay-rich lake sediments. These phases are paramagnetic at room temperature and become ferromagnetic at low temperature. The presence of these phases is further supported by the HT measurements that show a gradual increase in magnetic moment between 300°C and 500°C (Figure 1b), probably due to the transformation of these phases to magnetite. The diverse magnetic mineral phases in clay-rich lake sediments could result from the fact that detritus came from broad source areas while the ice front retreated.

Marl sediments appear as a transitional zone between clays and gyttja. The magnetic properties also tend to display a transition in magnetic behavior. From the deepest to the shallowest marl in the core, LT experiments indicate that the Verwey transition gradually becomes less pronounced in the warming curves. However, the Verwey transition remains recognizable in cooling curves (Figure 2a), suggesting the presence of magnetite. HT experiments tend to display a transition in magnetic behavior as well. Magnetic moment of marls just above clay shows a sharp increase while temperature drops across ~300°C, suggesting some contribution from iron sulphides, probably pyrrohtite. Marls just below the gyttja, however, display a gradual

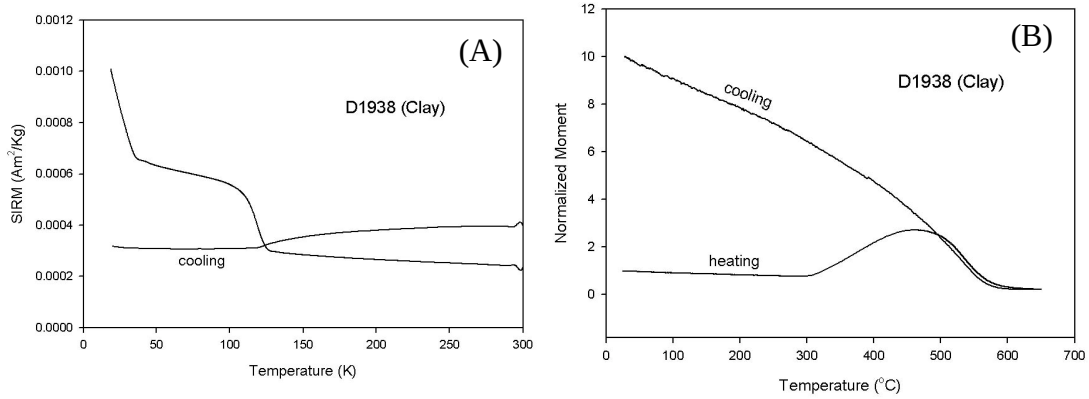

Figure 1. Low temperature (a) and high temperature (b) properties of the clay-dominated sediments. The sample acquired SIRMs in a 2.5T field at 20K (and 300K) prior to the warming (cooling) process.

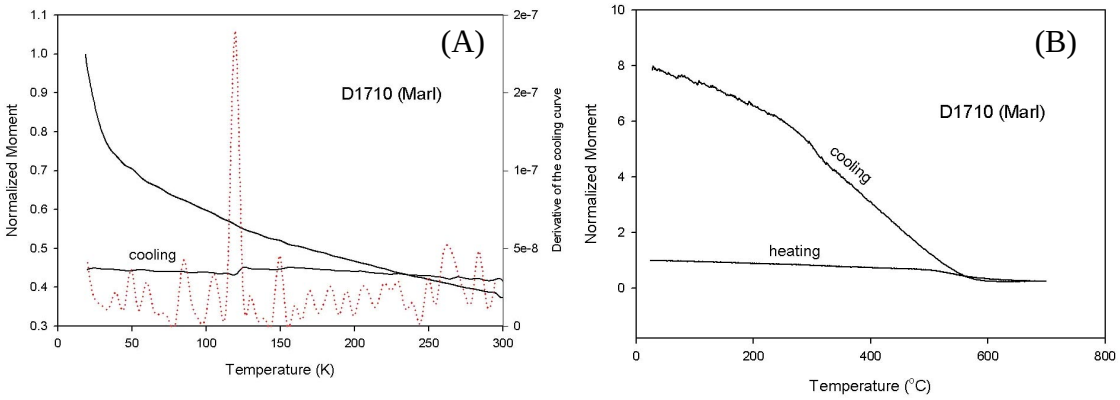

Figure 2. Low temperature (a) and high temperature (b) behaviors of a marl sample. The dash line is the derivative of the cooling curve. The spike at ~120K is interpreted as a Verwey transition indicating the presence of magnetite.

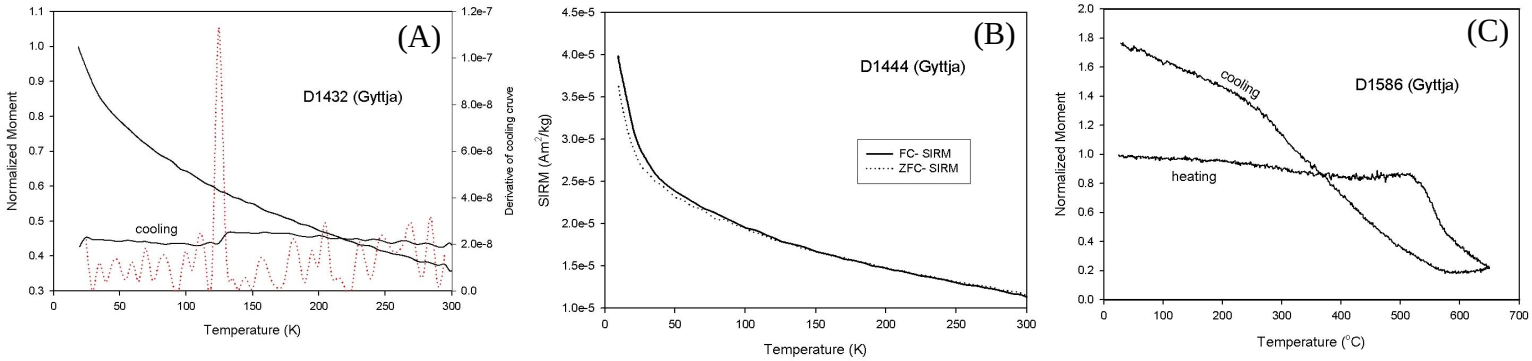

Figure 3. Magnetic properties of gyttja samples. (a) the Verwey transition indicates the presence of magnetite; (b) thermal demagnetization of SIRMs acquired in zero-field cooling (ZFC) and field cooling (FC) show almost no difference in the loss of SIRM around 100K, suggesting that magnetite particles are probably not biogenic (Moskowitz et al., 1993); (c) the magnetic moment increased after thermal treatment, although the magnitude of increase is less than that of the marl- and clay-dominated samples.

increase in magnetic moment while temperature decreased from 700°C (Figure 2b), indicating virtually no contribution from iron sulphides. Siderite was considered an important magnetic phase that may occur in the marl. The zero field cooling and field cooling (ZFC/FC) experiments did not show a phase transition at ~38K, diagnostic of the presence of siderite (Housen et al., 1996). The transition in magnetic properties of marl sediments may be associated with climate change during the late Pleistocene-early Holocene, when cold climate is gradually taken over by warm climate.

Gyttja accounts for the top half of the core and contains up to ~80% organic materials. The magnetization of gyttja is generally very weak. The LT measurements of all gyttja samples showed no phase transitions in the warming curves, but the cooling curves did show a faint transition at ~120K, which is more prominent in the derivative of a cooling curve (Figure 3a). This transition is interpreted to indicate magnetite particles in gyttja. The ZFC/FC data neither showed a phase transition at ~38 K, diagnostic of pyrrhotite (Dekkers et al., 1989), nor exhibited a differential loss in SIRM at ~110 K (Figure 3b) to suggest a biogenic origin of magnetite (Moskowitz et al., 1993). High temperature thermomagnetic curves often show a gradual increase in magnetic moment during cooling (Figure 3c). This gradual increase in magnetic moment implies that non-magnetic phases probably have been transformed into magnetic minerals.

The magnetic susceptibility of gyttja is very weak and the high temperature susceptibility measurements yielded almost only the sample holder's susceptibility. The signal/noise ratios for most gyttja samples are too low to identify magnetic minerals from their characteristic Curie temperatures. Only a handful of samples showed an overall susceptibility variation pattern that appears to be consistent with their high temperature thermomagnetic curves. The hysteresis loop results show that MD grains dominate the clay-rich sediments; whereas marl and gyttja are dominated by PSD grains (Figure 4). Although the Day plot shows that both marl and gyttja are indistinguishably dominated by PSD grains, a difference in magnetic grain size between the marl and gyttja may exist because a PSD interpretation in a Day plot could also be due to a mixture of MD grains and SD/SP grains in varying proportions.

The weak room temperature magnetization of gyttja and extensive mineralogical alteration during high temperature experiments make the interpretation of its magnetic properties difficult. Detailed interpretation of the minor variations in magnetic properties of the gyttja will need the precise chronology data and magnetic data from other cores. At present, both ^{14}C dating and the magnetic data of the shallow core are still in progress. When these datasets are available, the intra-lake correlation and inter-lake correlation with other independent climatic proxies will be made and should shed light on the possible magnetic mineral – climate link in organic rich sediments. The magnetic results of the deep core obtained at the IRM will provide the crucial magnetic mineralogical constraints for the upcoming detailed interpretation.

Acknowledgements

I would like to thank the IRM personnel for their kind and timely help during my visit. Discussions with Mike, Qingsong, and Christoph Geiss helped interpretation of the results.

References

Dekkers, M.J., Mattei, J.L., Fillion, G., and Rochette, P., 1989. Grain size dependence of the magnetic behavior of pyrrhotite during its low-temperature transition at 34k. *Geophysical Research Letters* 16, 855-858.

Housen, B.A., Banerjee, S.K., and Moskowitz, B.M. 1996. Low-temperature magnetic properties of siderite and magnetite in marine sediments. *Geophysical Research Letters* 23, 2843-2846.

Moskowitz, B.M., Frankel, R.B., and Bazylinski, D.A., 1993. Rock magnetic criteria for the detection of biogenic magnetite. *Earth and Planetary Science Letters* 120, 283-300.

Verwey, E.J. 1939. Electronic conduction of magnetite (Fe_3O_4) and its transition point at low temperatures. *Nature* 144, 327-328.

VF Reports

continued on p. 7...

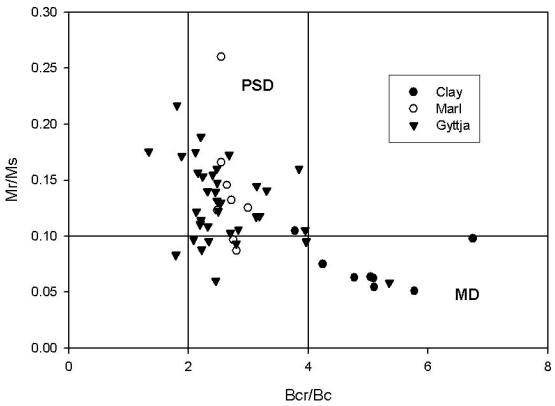

Figure 4. Hysteresis loop parameters used to estimate grain size. Mr=saturation remanence; Ms=saturation magnetization; Bcr=coercivity of remanence; Bc=coercivity.

The "Acquedotto Claudio" was initiated by Caligola in 38 AD and completed by Claudius in 52 AD (it was likely active already in 47 AD). The acqueduct had a total length of ca. 69 km, the last 9.5 km of which were built over arches (the initial part was underground). The acqueduct is relatively well preserved. Here the height ~17 m and the distance between pillars is 5.5 m. The pillars are made of local tuff blocks (volcanic products from the Alban Hills), slightly cemented. (photo by Leonardo Sagnotti).

Current Abstracts

A list of current research articles dealing with various topics in the physics and chemistry of magnetism is a regular feature of the IRM Quarterly. *Articles published in familiar geology and geophysics journals are included; special emphasis is given to current articles from physics, chemistry, and materials-science journals. Most abstracts are culled from* INSPEC *(© Institution of Electrical Engineers),* Geophysical Abstracts in Press *(© American Geophysical Union), and* The Earth and Planetary Express *(© Elsevier Science Publishers, B.V.), after which they are subjected to Procrustean editing and condensation for this newsletter. An extensive reference list of articles (primarily about rock magnetism, the physics and chemistry of magnetism, and some paleomagnetism) is continually updated at the* IRM. *This list, with more than 5200 references, is available free of charge. Your contributions both to the list and to the Abstracts section of the* IRM Quarterly *are always welcome.*

Alteration & Remagnetization

Madsen, K. N., Walderhaug, H. and Torsvik, T., 2002, **Erroneous fold tests as an artifact of alteration chemical remanent magnetization**: *Journal of Geophysical Research, v.107*, no.B12, 2369.
A laboratory CRM experiment performed on a Silurian lava, with a well-defined single component NRM carried by deuterically oxidized titanomagnetite (TM), shows that the CRM acquired has an orientation between parent phase NRM and remagnetizing field. Stepwise unfolding of the CRM gave a syntectonic fold test result. The variation of remanence deflection with angle between H_{CRM} and initial NRM can be understood in terms of vector addition of fields or remanence components.

Gillett, S. L., 2003, **Paleomagnetism of the Notch Peak contact metamorphic aureole, revisited: Pyrrhotite from magnetite plus pyrite under submetamorphic conditions**: *Journal of Geophysical Research-Solid Earth, v.108*, no.B9, 2446.
A scattered, two-polarity remagnetization is now thought to reside in metamorphic pyrrhotite, formed in part by in-situ reduction of magnetite by pyrite and organic compounds. Isotopic evidence rules out large-scale introduction of reducing fluids. At higher grades, some pyrrhotite probably also formed by the reaction of pyrite and Fe-bearing silicates. Pyrrhotite formation in rocks that are not obviously metamorphosed shows that the reactions could proceed at very low (<200°C) temperatures, the feasibility of which is shown by detailed thermodynamic calculations

Urbat, M. and Brandau, A., 2003, **Magnetic properties of marine sediment near the active Dead Dog Mound, Juan de Fuca Ridge, allow to refine hydrothermal alteration zones**: *Physics & Chemistry of the Earth, v.28*, no.16-19, p.701-709.
Ubiquitous trace magnetic minerals in these marine sediments are highly sensitive to both temperature and fluid induced post-depositional alteration, allowing for a refined definition of the lithological alteration zones as well as the establishment of additional lateral hydrothermal fluid flow.

Anisotropy

Fawcett, T. C., Burmester, R. F., Housen, B. A. and Iriondo, A., 2003, **Tectonic implications of magnetic fabrics and remanence in the Cooper Mountain pluton, North Cascade Mountains, Washington**: *Canadian Journal of Earth Sciences, v.40*, no.10, p.1335-1356.
The magnetic foliation in this pluton typically has a steep dip and a northwest strike; the magnetic lineation plunges moderately to shallowly northwest or southeast. The NRM, measured to evaluate post-emplacement tilt, has two components carried by pyrrhotite and magnetite. The paleomagnetic results and ~47 Ma Ar^{40}-Ar^{39} ages suggest that there has been no remagnetization or significant reorientation of the pluton since emplacement.

Hus, J. J., 2003, **The magnetic fabric of some loess/ palaeosol deposits**: *Physics & Chemistry of the Earth, v.28*, no.16-19, p.689-699.
The AMS of deposits from Asia, Europe and Siberia all have a bedding-parallel foliation with low lineation. Lineations in the upper part of the Wucheng formation show a preferential (prevailing palaeowind?) direction. Soil formation results in decreasing degree of anisotropy and foliation, and in some cases in large deviations of the principal susceptibility directions caused by bioturbation. The AMS reflects both crystallographic alignment of phyllosilicates and shape alignment of MD magnetites.

Zhou, Y., Wu, S. M., Qiu, X. L. and Zhou, P., 2003, **Study on finite strain and its relationship with magnetic fabric along Ailao Shan-Red River shear zone**: *Journal of Geophysical Research-Solid Earth, v.108*, no.B10, 2479.
Shear strains vary greatly here; ellipticity of amygdules in basalt ranges from 6.79 to 10.47 (corresponding shear strain γ_{xz} = 2.22-2.93), and ellipticity of garnets from 1.56 to 2.95 (γ_{xz} = 0.45-1.14) in core gneiss. Ferromagnetic minerals (mainly PSD and MD Ti-poor magnetite) and hornblende dominate the AMS. A poor axial ratio correlation between the magnetic and strain ellipsoids suggests that the finite strain cannot be evaluated using the magnetic fabric when the latter is a combined result from multiple minerals.

Data Processing and Analysis

Borradaile, G. J. and Hamilton, T., 2003, **Limestones distinguished by magnetic hysteresis in three-dimensional projections**: *Geophysical Research Letters, v.30*, no.18, 1973.
We show that limestone samples are simply discriminated in a new 2D projection produced by projecting hysteresis data from three dimensions (x, y, z = M_r/M_s, B_{cr}, B_c) onto a plane containing the M_r/M_s axis. The orientation of the plane is controlled by its x-axis that is defined by a suitably selected B_{cr}/B_c ratio, most often in the magnetite PSD range, $2 < (B_{cr}/B_c) < 4$.

Fabian, K., 2003, **Some additional parameters to estimate domain state from isothermal magnetization measurements**: *Earth & Planetary Science Letters, v.213*, no.3-4, p.337-345.
For quantitative analysis of domain state, four new isothermal magnetization parameters are proposed. A hysteresis shape parameter and a coercivity ratio can be directly calculated from standard hysteresis and backfield measurements. A transient energy dissipation ratio and the viscosity of IRM, require additional measurements, which, however, do not increase measurement time noticeably. The effectiveness of these parameters is discussed theoretically and demonstrated experimentally.

Environmental Magnetism and Paleoclimate Proxies

Chen, T. H., *et al.*, 2003, **Formation mechanism of ferromagnetic minerals in loess of China: TEM investigation**: *Chinese Science Bulletin, v.48*, no.20, p.2259-2266.
Primary magnetite has the morphology and surface characteristics of eolian detrital particles. High-Ti and low-Ti magnetite may be derived from magmatic and metamorphic rocks, respectively. Nanometer-scale imaging shows partial pedogenic alteration of primary detrital magnetite to pseudomorphic maghemite. Some nanometer scale magnetite or maghemite particles also formed by pedogenic alteration of chlorite. These contain a small amount of P and S, which is the signal of microbe-mineral interaction.

Hanesch, M., Scholger, R. and Rey, D., 2003, **Mapping dust distribution around an industrial site by measuring magnetic parameters of tree leaves**: *Atmospheric Environment, v.37*, no.36, p.5125-5133.
We sampled maple leaves at 102 locations in and around Leoben and determined κ, IRM at 1 Telsa, the S-ratio (IRM_{-100mT}/IRM_{1T}) and the ratio IRM/κ. The results showed that one soft ferrimagnetic phase is dominant over the whole investigated area. This finding was corroborated by SEM analysis of the leaves. A soil κ map shows the same spatial pattern, indicating that the location of the main source has been the same over a long time span.

Hu, S., *et al.*, 2003, **Magnetic responses to acidification in Lake Yangzonghai, SW China**: *Physics & Chemistry of the Earth, v.28*, no.16-19, p.711-717.
A power plant built in 1960 is close to the lake, and coal ashes can be found within the uppermost 12 cm of sediment. Ash collected directly from the power plant is strongly magnetic, and its main magnetic content is magnetite. However, χ and ARM are very low in the upper 12 cm. Al, a sensitive indicator for acidification, decreases above 10 cm, and some acidophile diatom species show the reverse pattern. Thus the lake was acidified after the power plant was built, which caused dissolution of magnetic particles.

Kapicka, A., Jordanova, N., Petrovský, E., and Podrázský, V., 2003, **Magnetic study of weakly contaminated forest soils**: *Water, Air, and Soil Pollution v.148*, p. 31–44.
Magnetic and magnetomineralogical studies show weak contamination in the uppermost layer of forest soils from Krkonoše (Giant Mountains) National Park in the Czech Republic. Thermomagnetic analysis, acquisition of remanence, AF demagnetization of SIRM and χ_{fd} were measured in bulk samples and magnetic extracts. XRD and SEM were used to identify ferrimagnetic fractions.

Kissel, C., Laj, C., Clemens, S. and Solheid, P., 2003, **Magnetic signature of environmental changes in the last 1.2 Myr at ODP site 1146, South China Sea**: *Marine Geology, v.201*, no.1-3, p.119-132.
A precise age model based on magnetostratigraphy and ^{18}O shows that the studied interval extends to 1.18 Myr. Long-term and short-term variations have been documented in the magnetic parameters. Except for the most recent 200 kyr, where the pattern changes, cold/warm periods coincide with low/high magnetic content, and magnetic grains are coarser during cold stages and finer during warm periods. This illustrates changes in the balance between dominant winter and summer monsoon activity.

Liu, Q. S., *et al.*, 2003, **An integrated study of the grain-size-dependent magnetic mineralogy of the Chinese loess/ paleosol and its environmental significance**: *Journal of Geophysical Research-Solid Earth, v.108*, no.B9, 2437.
Magnetic extracts were divided into two size fractions by gravitational settling. Hysteresis, low- temperature remanence, SEM and XRD studies show that the loess coarse particles are MD magnetite with slight oxidation; paleosol coarse particles are also MD magnetite but with a higher oxidation degree; loess fine particles are PSD magnetite with a high oxidation degree; and paleosol fine particles are PSD maghemite. Single domain (SD) and superparamagnetic (SP) maghemite mainly stay in the residues.

Liu, X. M., Rolph, T., An, Z. S. and Hesse, P., 2003, **Paleoclimatic significance of magnetic properties on the Red Clay underlying the loess and paleosols in China**: *Palaeogeography Palaeoclimatology Palaeoecology, v.199*, no.1-2, p.153-166.
This widespread Miocene-Pliocene (7.2-2.5 Ma) aeolian deposit comprises highly-developed soils and interbedded layers of reddish loess-like material, interpreted to represent climatic fluctuations. Magnetite, maghemite and hematite (and possibly goethite) are present, and there are good correlations among χ, SP content, and Rb:Sr ratio, an independent weathering index. More work to deconvolve the climatic record of the Red Clay may extend the record of

paleomonsoon evolution back into the late Miocene.

Muxworthy, A. R., Matzka, M., Davila, A. F. and Petersen, N., 2003, **Magnetic signature of daily sampled urban atmospheric particles**: *Atmospheric Environment, v.37*, no.29, p.4163-4169.
In samples collected in Munich over a 160-day period, mass-dependent magnetic parameters varied in a complicated way governed by both the meteorological conditions and the particulate matter (PM) loading rate, whereas mineralogy/ grain-size-dependent parameters displayed little variation. The signal was dominated by fine (<100 nm) magnetite-like grains thought to be derived primarily from vehicles. Such small grains are particularly dangerous to humans. There was also evidence that the magnetite-like grains were covered with an oxidised rim.

Oldfield, F., *et al*., 2003, **The late-Holocene history of Gormire Lake (NE England) and its catchment: a multiproxy reconstruction of past human impact**: *Holocene, v.13*, no.5, p.677-690.
Magnetic measurements, XRF and organic biogeochemical analyses provide evidence for changes in sediment composition and source and for catchment erosion over the last 3500 years. Interpretation of the magnetic record is complicated by the presence of biogenic magnetite and authigenic greigite and by probable magnetite dissolution. Magnetic indications of catchment erosion are nevertheless clearly distinguishable, especially in the record of the antiferromagnetic minerals haematite and goethite.

Retallack, G. J., Sheldon, N. D., Cogoini, M. and Elmore, R. D., 2003, **Magnetic susceptibility of early Paleozoic and Precambrian paleosols**: *Palaeogeography Palaeoclimatology Palaeoecology, v.198*, no.3-4, p.373-380.
In deposits pre-dating the evolution of rooted land plants, root traces cannot be used for recognizing paleosols. Magnetic susceptibility peaks are useful supporting evidence for paleosols that are red and oxidized, but not for those with reduction spots, iron-manganese nodules or other evidence of gleization. These ancient paleosols have much lower χ than comparable Quaternary units, due in part to burial recrystallization of fine-grained ferrimagnets, and in part to a lower level of susceptibility-enhancing microbial activity.

Watkins, S. J. and Maher, B. A., 2003, **Magnetic characterisation of present-day deep-sea sediments and sources in the North Atlantic**: *Earth & Planetary Science Letters, v.214*, no.3-4, p.379-394.
North Atlantic surface-sediment magnetic data show distinct spatial patterns related to sediment sources and transport pathways, especially of windblown dust and ice-rafted debris (IRD). The spatial distributions of the IRD-dominated sediments substantiate those mapped previously using lithological tracers, provide additional spatial information on sediment sources and pathways, and suggest that deep water currents are less significant than proposed in controlling present-day sediment mineralogy and distribution.

Xiong, S. F., *et al.*, 2002, **Northwestward decline of magnetic susceptibility for the red clay deposit in the Chinese Loess Plateau**: *Geophysical Research Letters, v.29*, no.24, 2002GL015808.
Magnetic susceptibility in the Miocene-Pliocene red clay deposits shows a clear systematic decrease from the southeast (Lingtai section) to the northwest (Baishui section). This suggests that the climatic controls (probably precipitation) had a northwestward-decreasing gradient during the red clay deposition, similar to the present pattern, implying that the influence of the East Asian summer monsoon on the Chinese Loess Plateau has persisted from at least 6 Ma.

Extraterrestrial Magnetism

Barber, D. J. and Scott, E. R. D., 2003, **Transmission electron microscopy of minerals in the martian meteorite Allan Hills 84001**: *Meteoritics & Planetary Science, v.38*, no.6, p.831-848.
TEM, X-ray microanalysis, and electron diffraction show magnetite crystals that are epitaxially oriented at voids and microfractures, clearly formed in situ. Fully embedded, faceted magnetites are topotactically oriented on carbonate so that their oxygen layers are aligned. All magnetite and periclase crystals probably formed by exsolution from carbonate following impact-induced thermal decomposition. Any magnetites that existed in the rock before shock heating could not have preserved evidence for biogenic activity.

Brearley, A. J., 2003, **Magnetite in ALH 84001: An origin by shock-induced thermal decomposition of iron carbonate**: *Meteoritics & Planetary Science, v.38*, no.6, p.849-870.
TEM studies show that the carbonate fragments embedded within feldspathic glass contain myriad, nanometer-sized magnetite particles with cuboid, irregular, and teardrop morphologies, frequently associated with voids. The fragments of carbonate must have been incorporated into the melt at temperatures of ~900°C, well above the upper thermal stability limit of siderite. These observations suggest that most, if not all, of the fine-grained magnetite associated with Fe-bearing carbonate in ALH 84001 could have been formed as result of the thermal decomposition of the siderite and is not due to biological activity.

Catling, D. C. and Moore, J. A., 2003, **The nature of coarse-grained crystalline hematite and its implications for the early environment of Mars**: *Icarus, v.165*, no.2, p.277-300.
The Mars Global Surveyor spacecraft has detected deposits of coarse-grained, gray crystalline hematite in Sinus Meridiani, Aram Chaos, and Vallis Marineris. The topography and the collapsed nature of the chaotic terrain favor a hydrothermally charged aquifer as the original setting where the hematite formed. The coexistence of factors required to form the gray hematite deposits would also have produced a favorable environment for primitive life, including liquid water, electron donors (H_2), and electron acceptors (Fe^{3+}).

Kopp, R. E. and Humayun, M., 2003, **Kinetic model of carbonate dissolution in Martian meteorite ALH84001**: *Geochimica et Cosmochimica Acta, v.67*, no.17, p.3247-3256.
The magnetites and sulfides in the rims of carbonate globules in ALH84001 have been claimed as evidence of past life on Mars. Model calculations indicate that the rims could have formed in < 50 yr of exposure to small amounts of aqueous fluids at ambient temperatures, more likely in the modern Martian or terrestrial atmospheres than in an ancient Martian atmosphere. A terrestrial origin is supported by anticorrelated variations of radiocarbon with $\delta^{13}C$, indicating solution-precipitation reactions immediately after initial fall (~13,000 yr ago) and again during recent exposure prior to collection.

McKay, C. P., Friedmann, E. I., Frankel, R. B. and Bazylinski, D. A., 2003, **Magnetotactic bacteria on Earth and on Mars**: *Astrobiology, v.3*, no.2, p.263-270.
There are credible arguments for both the biological and non-biological origin of the magnetite in ALH84001, and we suggest that more studies of ALH84001, extensive laboratory simulations of non-biological magnetite formation, as well as further studies of magnetotactic bacteria on Earth will be required to further address this question. Magnetite grains produced by bacteria could provide one of the few inorganic traces of past bacterial life on Mars that could be recovered from surface soils and sediments.

Newsom, H. E., *et al.*, 2003, **Paleolakes and impact basins in southern Arabia Terra, including Meridiani Planum: Implications for the formation of hematite deposits on Mars**: *Journal of Geophysical Research-Planets, v.108*, no.E12, 8075.
Our discovery of a chain of paleolake basins and channels along the southern margin of the hematite deposits in Meridiani Planum supports the possible role of water in the formation of the hematite and other layered materials in the region. The hematite may have formed by direct precipitation from lake water, as coatings precipitated from groundwater, or by oxidation of preexisting iron oxide minerals. Stratigraphic relationships indicate that the formation of channels in the region occurred over much of Mars' history.

Treiman, A. H., 2003, **Submicron magnetite grains and carbon compounds in martian meteorite ALH84001: Inorganic, abiotic formation by shock and thermal metamorphism**: *Astrobiology, v.3*, no.2, p.369-392.
We propose that the carbonate globules in ALH84001 were deposited from hydrothermal water, without biological mediation. Thereafter, an impact shock event raised its temperature nearly instantaneously to 500-700K, decomposing Fe-rich carbonate and producing magnetite and other minerals. Carbon-bearing gas from the carbonate decomposition reacted with water to produce organic matter via Fischer-Tropsch-like reactions, catalyzed by the magnetite.

Magnetic Field Records and Paleointensity Methods

Dunlop, D. J. and Yu, Y. J., 2003, **Testing an inverse Thellier method of paleointensity determination**: *Journal of Geophysical Research-Solid Earth, v.108*, no.B9, 2447.
Inverse TRM (ITRM) can be produced in nature if a magnetite-bearing meteorite warms through the Verwey transition (T_V = 120 K) in the Earth's field. A new inverse Thellier method of paleointensity determination uses cooling-heating steps below room temperature T_0. In our experiments, NRM was an ITRM produced by warming from 30 K to T_0, for magnetites of 0.065, 0.2, 1, 3, 6, 9, 17, 20 and 135 µm and two gabbros containing elongated SD magnetite. SD samples had quasi-linear inverse Arai plots but other samples had convex-down curves, resembling Arai plots for TRM in MD grains. However, the inverse Thellier method may have more linear behavior if the NRM is a TRM because the greater resistance of TRM to LTD should offset the too-rapid decay of ITRM in zero-field steps.

Frank, U., Schwab, M. J. and Negendank, J. F. W., 2003, **Results of rock magnetic investigations and relative paleointensity determinations on lacustrine sediments from Birkat Ram, Golan Heights (Israel)**: *Journal of Geophysical Research-Solid Earth, v.108*, no.B8, 2379.
Relative paleointensity (RPI) was estimated by normalizing the NRM intensity after demagnetization at 20 mT ($J_{NRM(20\ mT)}$) by different concentration parameters. The MDF of the NRM is coherent with the RPI estimates, indicating that a sedimentary effect has not sufficiently been removed. The RPI variation, however, correspond to archeomagnetic records from Bulgaria and Greece. A second normalization, based on the linear relationship between RPI and MDF(NRM), improved the records.

Krasa, D., Heunemann, C., Leonhardt, R. and Petersen, N., 2003, **Experimental procedure to detect multidomain remanence during Thellier-Thellier experiments**: *Physics & Chemistry of the Earth, v.28*, no.16-19, p.681-687.
A new reliability test detects the presence of MD particles by verifying the law of additivity of pTRMs. Additivity holds for regular pTRMs (i.e. cooling from T_c to T_1) for both SD and MD particles, whereas it fails for pTRM* (heating from 20°C to T_1) in the case of MD particles. Thellier experiments, based on pTRM*, fail with MD carriers. Experiments covering the grain size range 23 nm to 12.1 µm show a significant error for all samples with grain sizes >0.7 µm, but our experiment is able to detect this failure.

Kruiver, P. P., Krijgsman, W., Langereis, C. G. and Dekkers, M. J., 2002, **Cyclostratigraphy and rock-magnetic investigation of the NRM signal in late Miocene palustrine-alluvial deposits of the Librilla section (SE Spain)**: *Journal of Geophysical Research, v.107*, no.B12, 2334.
A refined magnetostratigraphy shows that the sedimentary cycles reflect climatic precession. Two intervals of complex NRM behavior were identified, showing normal and reversed overprints. Fuzzy c-means cluster analysis on a geochemical data yields a three-cluster model that roughly describes lithology. Remarkably, all the samples with a normal overprint belong to one particular cluster. The reversed overprints, however, do not show any relation to the cluster partition.

Magnetic Microscopy and Spectroscopy

Kasama, T., Golla-Schindler, U. and Putnis, A., 2003, **High-resolution and energy-filtered TEM of the interface between hematite and ilmenite exsolution lamellae: Relevance to the origin of lamellar magnetism**: *American Mineralogist, v.88*, no.8-9, p.1190-1196.
The interfaces between fine-scale exsolution lamellae have been studied by TEM, to investigate the lamellar magnetism hypothesis for the unusual properties of an igneous rock from Rogaland, Norway. The interfaces between the coarse hematite and ilmenite lamellae (length >1 µm) and their hosts have some interface dislocations to relieve elastic coherency strain, but very fine lamellae (length <50 nm) have no interface dislocations and are perfectly coherent. These results are in accord with the predictions of Monte Carlo simulations of the exsolution process and with the hypothesis that coherent and sharp structural and compositional interfaces are the origin of lamellar magnetism.

Kawakami, T., *et al.*, 2003, **Mössbauer spectroscopy of pressure-induced phase transformation from maghemite to hematite**: *Journal of the Physical Society of Japan, v.72*, no.10, p.2640-2645.
Using a diamond anvil cell, ^{57}Fe Mössbauer spectroscopy has been carried out on maghemite, γ-Fe_2O_3, under high pressure up to 30GPa. Maghemite transforms to hematite, α-Fe_2O_3, with a wide coexistent pressure range. The onset of phase transformation is 14 GPa and complete transformation to hematite is found at 26GPa. The pressure-induced transformation is irreversible and hematite is preserved at decompression process. The magnetization direction stays nearly parallel after maghemite transforms to hematite. This strong orientation of magnetization does not appear on compression of original hematite, and is therefore due to the transformation.

Klausen, S. N., *et al.*, 2003, **An inelastic neutron scattering study of hematite nanoparticles**: *Journal of Magnetism & Magnetic Materials, v.266*, no.1-2, p.68-78.
Neutron scattering studies in nanocrystalline hematite at temperatures from 5 to 325 K show that the particles are canted antiferromagnetic (weakly ferromagnetic) at temperatures at least down to 5 K. The data and their temperature dependence can with good agreement be interpreted on the basis of the Neel-Brown theory for superparamagnetic relaxation and a model for the collective magnetic excitations.

Sandhu, A., Masuda, H. and Oral, A., 2003, **Room temperature scanning micro-Hall probe microscopy under extremely large pulsed magnetic fields**: *IEEE Transactions on Magnetics, v.39*, no.5 Part 2, p.3462-3464.
The versatility of a room-temperature scanning Hall probe microscope system with an integrated minicoil capable of generating pulsed magnetic fields up to 2.9 T was demonstrated by imaging magnetic structures on the surface of 1.4-MB floppy disks. Vibration isolation between the sample and minicoil enabled extremely fast measurements, using a GaAs-AlGaAs micro-Hall probe sensor located at a height of 0.5 µm above-the sample surface.

Magnetic Petrology and Anomaly Sources

Alva-Valdivia, L. M., *et al.*, 2003, **Integrated magnetic studies of the El Romeral iron-ore deposit, Chile: implications for ore genesis and modeling of magnetic anomalies**: *Journal of Applied Geophysics, v.53*, no.2-3, p.137-151.
CRM seems to be present in most of investigated ore and wall-rock samples, substituting completely or partially the original TRM. Magnetite (or Ti-poor titanomagnetite) and

continued on p. 6...

titanohematite are commonly found in the ores. Magmatic titanomagnetite, found in igneous rocks, shows trellis texture, which is compatible with high temperature (deuteric) oxy-exsolution processes. Hydrothermal alteration in ore deposits is indicated by goethite and hematite oxide minerals.

Arkani-Hamed, J., 2003, **Thermoremanent magnetization of the Martian lithosphere**: *Journal of Geophysical Research-Planets, v.108*, no.E10, 5114.
This model assumes that the upper part of the lithosphere acquired TRM early in Mars' history in the presence of a core field, whereas the lower part has been gradually magnetized by the magnetic field of the upper part as it has cooled below T_C. If the Martian lower lithosphere is more magnetic than Earth's, e.g., by an order of magnitude, the secondary magnetization can be significant, although still weaker than the primary magnetization of the upper part. In all models considered the primary magnetization is ~20-30 A/m and has the dominant contribution to the observed magnetic anomalies.

Gac, S., Dyment, J., Tisseau, C. and Goslin, J., 2003, **Axial magnetic anomalies over slow-spreading ridge segments: insights from numerical 3-D thermal and physical modelling**: *Geophysical Journal International, v.154*, no.3, p.618-632.
The axial magnetic anomaly along Mid-Atlantic Ridge segments is systematically twice as high at segment ends compared with segment centres, due to: (1) shallower Curie isotherm at segment centres, (2) higher Fe-Ti content at segment ends and/or (3) serpentinized peridotites at segment ends. 3-D numerical modeling suggests that, in the case of aligned and slightly offset segments, a combination of (2) and (3) dominate; for greater offsets, serpentinized peridotites at segment ends can account for the observations.

Magnetization & Demagnetization Processes

Ozima, M. and Funaki, M., 2003, **Hemoilmenite as a carrier of SRTRM in dacitic pumice from Akagi, Ontake and Sambe Volcanoes, Japan**: *Earth & Planetary Science Letters, v.213*, no.3-4, p.311-320.
Dacite pumice samples from Akagi Volcano acquire an intense self-reversed TRM (SRTRM). Bitter patterns of the oriented hemoilmenite crystals from both the Haruna and Akagi volcanoes indicate that ordered ferrimagnetic and disordered weak-ferromagnetic phases are inter-grown in relatively comparable amounts, with an irregular texture. This pattern is consistent with rapid quenching of these pumices. We conclude that not only the chemical composition of the hemoilmenite, but also the cooling rate control SRTRM acquisition.

Spassov, S., *et al.*, 2003, **A lock-in model for the complex Matuyama-Brunhes boundary record of the loess/palaeosol sequence at Lingtai (Central Chinese Loess Plateau)**: *Geophysical Journal International, v.155*, no.2, p.350-366.
The MBB at Lingtai occurs in L8 and is characterized by multiple polarity flips. The NRM is mainly carried by two coexisting phases, one with higher coercivity (dominant in loess layers and thought to be detrital), and one with lower coercivity (prevailing in palaeosols and probably formed in situ by (bio-)chemical processes). A dual lock-in model, with the harder component physically locked shortly after deposition, and the softer component locking chemically at greater depth, is able to explain the observed rapid multiple polarity flips and low magnetization intensities as well as the stratigraphic shift of the Lingtai MBB with respect to the marine records.

Walton, D., 2002, **Conditions for ferromagnetic resonance in nanoparticles and microwave magnetization**: *Geophysical Research Letters, v.29*, no.24, 2002GL016049.
Microwaves are absorbed by generating spin-waves, a very efficient way to raise the temperature of ferromagnetic particles in a non-magnetic matrix. Since microwaves are essentially only absorbed by the magnetic grains the matrix remains cool which eliminates the problem of mineral alteration. A key factor is the size of the magnetic particles. Spin waves whose wavelength exceeds about twice the size of the particle are not possible so the dispersion relations for small particles are cutoff at the corresponding wave-vector.

Yu, Y., Dunlop, D. J. and Ozdemir, O., 2003, **Testing the independence law of partial ARMs: implications for paleointensity determination**: *Earth and Planetary Science Letters, v.208*, (1-2), p. 13-26.
The independence of pARMs was tested by AF demagnetizing orthogonal pARMs whose blocking field intervals do not overlap with each other. Experimentally the two pARMs demagnetized independently for SD grains but not for MD and PSD grains. Experimentally and in numerical simulations, when a total ARM (simulating primary remanence in a field H_a) was orthogonally overprinted by pARM (simulating remagnetization in H_b), estimation of the intensity of H_b was relatively successful but the intensity of H_a was always underestimated. Conversely, the direction of H_a was preserved but the direction of H_b was spurious. These violation of pARM independence imply that the conventional criteria in pseudo-Thellier paleointensity determination require modification.

Yu, Y., Dunlop, D. J. and Ozdemir, O., 2003, **On the resolution of multivectorial remanences**: *Earth and Planetary Science Letters, v.208*, (1-2), p. 27-39.
In normalized vector plots of AF demagnetization of orthogonal pARMs, LTD-treated samples showed universal improvement in the degree of independence, greatest for synthetic SD and PSD magnetites and natural lake sediments, and to a lesser degree for synthetic MD magnetite, granites, and gabbros. In general, LTD provides a better resolution of superimposed vectors in multicomponent remanence. The direction of the original remanence is perfectly recovered. However, the pARM overprint is not perfectly resolved, especially for overprinting coercivities <40 mT, where the deviation is 10° or more.

Mineral & Rock Magnetism

Caizer, C., 2003, **Saturation magnetization of γ - Fe_2O_3 nanoparticles dispersed in a silica matrix**: *Physica B, v.327*, no.1, p.27-33.
M_S increases by 69.7% on cooling from 300 to 77 K for non-interacting nanoparticles of γ - Fe_2O_3 (0.68 vol%) isolated in an amorphous SiO_2 matrix. This is much higher than the corresponding increase for the bulk ferrite, which is only 9.5% in the same temperature range. We attribute the anomalous increase to low-T ferromagnetic ordering of a paramagnetic surface layer, with spins aligned by superexchange interaction. This amounts to an increase in the effective magnetic diameter of the particles from 10.20 to 11.76 nm at low temperatures.

Delius, H., Brewer, T. S. and Harvey, P. K., 2003, **Evidence for textural and alteration changes in basaltic lava flows using variations in rock magnetic properties (ODP Leg 183)**: *Tectonophysics, v.371*, no.1-4, p.111-140.
In subaerial basalts, χ and NRM are typically high in the altered flow top, and lower in the less-altered massive flow interior. In contrast, submarine lava flows typically display the opposite pattern. It is concluded that rate of cooling and degree of alteration are the main factors influencing the magnetization and, hence, the distribution of iron oxides.

Frederichs, T., von Dobeneck, T., Bleil, U. and Dekkers, M. J., 2003, **Towards the identification of siderite, rhodochrosite, and vivianite in sediments by their low-temperature magnetic properties**: *Physics & Chemistry of the Earth, v.28*, no.16-19, p.669-679.
Natural samples of siderite (FeCO3), rhodochrosite (MnCO3), and vivianite ([Fe3(PO4)2].8 H2O), authigenic sedimentary minerals that are paramagnetic at room temperature, were measured at low-T in an MPMS. Below their Neel temperatures, siderite (37 K) and rhodochrosite (34 K) acquire a strong spin-canted remanence (~0.4 Am^2/kg) from cooling in a 5 T magnetic field. Different ratios of FC and ZFC remanences allow a discrimination between the two minerals. Vivianite also shows metamagnetism below 5 K in 5 T fields and a 'two-stage' increase in susceptibility between 2 and 12 K attributed to successive short- and long-range magnetic ordering. Shifting of the Neel points to lower temperatures occurs with element substitution and non-stoichiometry, common in sedimentary environments.

Goya, G. F., Berquo, T. S., Fonseca, F. C. and Morales, M. P., 2003, **Static and dynamic magnetic properties of spherical magnetite nanoparticles**: *Journal of Applied Physics, v.94*, no.5, p.3520-3528.
Magnetic behavior of Fe_3O_4 nanoparticles changes with average particle size <d> from 5 to 150 nm. Bulk-like properties such as M_S, hyperfine parameters, H_C, and Verwey transition are observed in 150 nm particles. For decreasing particle size, T_V shifts down to ~20 K for <d>=50 nm and is no longer observable for smaller particles. The smallest particles (<d>=5 nm) display SP behavior at room temperature, with transition to a blocked state at T_B~45 K, which depends on the applied field. Dynamic ac susceptibility measurements show a thermally activated Arrhenius-Neel dependence of T_B on frequency for the 5 nm particles.

Gregorova, D., Hrouda, F. and Kohut, M., 2003, **Magnetic susceptibility and geochemistry of Variscan West Carpathian granites: implications for tectonic setting**: *Physics & Chemistry of the Earth, v.28*, no.16-19, p.729-734.
Granites usually display a bimodal distribution of χ, with modes on the order of 10^{-5}-10^{-4} SI and 10^{-3}-10^{-2} SI, respectively corresponding to ilmenite-bearing (S-type) and magnetite-bearing (I-type) granite. In the West Carpathians, isotope geochemistry discriminates an older peraluminous group (350-330 Ma) of two-mica granites and granodiorites, carrying monazite and ilmenite; and a younger metaluminous to subaluminous group (310-300 Ma) of biotite tonalites and granodiorites, carrying allanite and magnetite. Magnetic susceptibilities of both sets are in general rather low, on the order of 10^{-4}, in apparent contradiction with the granite origin as revealed geochemically. Unusual redox conditions controlled by the tectonic setting are possible explanations of this discrepancy.

Miranda, J. M., *et al.*, 2002, **Study of the Saldanha Massif (MAR, 36° 34 ' N): Constrains from rock magnetic and geophysical data**: *Marine Geophysical Researches, v.23*, no.4, p.299-318.
These basalt samples have magnetic minerals of SD grain size, typical of rapid cooling. Thermomagnetic study distinguishes between three different stages of low temperature oxidation: the presence of titanomagnetite, titanomagnetite and titanomaghemite, and exclusively of titanomaghemite. Based on established empirical relationships between T_C and degree of oxidation, the latter is tentatively deduced for all samples.

Peters, C. and Dekkers, M. J., 2003, **Selected room temperature magnetic parameters as a function of mineralogy, concentration and grain size**: *Physics & Chemistry of the Earth, v.28*, no.16-19, p.659-667.
A data set of room temperature magnetic parameters for iron oxides and sulphides, compiled from the literature, shows that hematite and in particular goethite are recognised by their high H_{CR}. The ratio M_{RS}/χ is high for pyrrhotite, intermediate for greigite and maghemite, and very low for (titano)magnetite. From the concentration-dependent parameters χ, M_{RS} and χ_{ARM}, χ displayed the least grain-size dependence, and is therefore the best indicator of concentration. All minerals except goethite showed a decrease in H_C and M_{RS}/M_S for d>1μm. Assessment of domain state was complicated by the similar properties of very small and large grains.

Mineral Physics & Chemistry

Cudennec, Y. and Lecerf, A., 2003, **Study of the formation processes of iron oxy-hydroxides; hypotheses of topotactic transformations**: *Comptes Rendus Chimie, v.6*, no.4, p.437-444.
Goethite, α-FeO(OH), is the most stable iron oxy-hydroxide. It can be formed directly from trivalent iron solutions or from 'white rust' $Fe(OH)_2$ by oxidation of divalent iron. Lepidocrocite, γ-FeO(OH), can be obtained at room temperature by fast oxidation of divalent iron in a 'green rust' precursor phase, containing also trivalent iron and chloride ions. Based on a structural study and a comparison of crystal structures of these different phases, we propose possible topotactic reactions.

Demianets, L. N., Pouchko, S. V. and Gaynutdinov, R. V., 2003, **Fe_2O_3 single crystals: hydrothermal growth, crystal chemistry and growth morphology**: *Journal of Crystal Growth, v.259*, no.1-2, p.165-178.
Optical and AFM study of the {h k i l} faces of hydrothermally-grown hematite single crystals show two main mechanisms of growth: layer-by-layer growth and island growth. Large flat terraces with height h 100-150 nm, width d ~10000 nm are observed on the {1 1 2 0} surface. Terraces are composed from steps of h~15-65, d~100-1200 nm, consisting of globules with rounded or elongated shapes and typical heights of 0.5-5 nm and lengths of 30-60 nm.

Froese, E., 2003, **Point defects in pyrrhotite**: *Canadian Mineralogist, v.41*, no.Part 4, p.1061-1067.
The nature of point defects in pyrrhotite can be determined from measurements of composition and the corresponding fugacity of S_2 by examining reaction equilibria written to involve perfectly ordered FeS, species deduced from point defects, and S_2. This approach is illustrated using the experimental data at 1257 K. In S-rich pyrrhotite, the predominant defect is produced by vacancies on Fe sites; in Fe-rich pyrrhotite, the predominant defect consists of Fe atoms on S sites.

Liu, H., *et al.*, 2003, **Static compression of α-Fe_2O_3: linear incompressibility of lattice parameters and high-pressure transformations**: *Physics & Chemistry of Minerals, v.30*, no.9, p.582-588.
Synchrotron-based XRD shows that α-Fe_2O_3 in a laser-heated diamond anvil cell remains in the corundum structure up to 50 GPa, but with a coexisting high-pressure phase above 45 GPa. Enhanced c-axis compressibility may lead to breaking of vertex- or edge-sharing bonds between octahedra, inducing the high-pressure phase transformation at 50 GPa. Analysis of linear compressibilities suggests that the high-pressure phase above 50 GPa is of the Rh_2O_3 (II) structure.

Pasternak, M. P., *et al.*, 2003, **Pressure-induced coordination crossover in magnetite; the breakdown of the Verwey-Mott localization hypothesis**: *Journal of Magnetism & Magnetic Materials, v.265*, no.2, p.L107-L112.
Temperature-dependent ^{57} Fe Mössbauer spectroscopy to 40 GPa shows that magnetite undergoes a coordination crossover (CC), whereby charge density is shifted from octahedral to tetrahedral sites and the spinel structure thus changes from inverse to normal with increasing pressure and decreasing temperature. The CC transition takes place almost exactly at the Verwey transition temperature (T_V = 122 K) at ambient pressure. While T_V decreases with pressure the CC-transition temperature increases with pressure, reaching 300K at 10GPa.

Sanders, J. P. and Gallagher, P. K., 2003, **Thermomagnetometric evidence of γ-Fe_2O_3 as an intermediate in the oxidation of magnetite**: *Thermochimica Acta, v.406*, no.1-2, p.241-243.
The oxidation of magnetite to hematite was followed by thermogravimetry (TG), both with and without a small magnetic field gradient imposed upon the sample. The results clearly indicate the formation of a strongly magnetic intermediate during oxidation, confirming the speculation that γ-Fe_2O_3 is an intermediate in this process.

van der Zee, C., Roberts, D. R., Rancourt, D. G. and Slomp, C. P., 2003, **Nanogoethite is the dominant reactive oxyhydroxide phase in lake and marine sediments**: *Geology, v.31*, no.11, p.993-996.
Reactive ferric oxides and oxyhydroxides are usually

quantified by selective chemical extractions that are not mineral specific. We have used cryogenic ^{57}Fe Mössbauer spectroscopy to show that the reactive iron oxyhydroxide phase in a large variety of lacustrine and marine environments is nanophase goethite (α-FeOOH), rather than the assumed surface-complex-stabilized, two-line ferrihydrite and accompanying mixture of clay and oxyhydroxide Fe-bearing phases.

Ziemniak, S. E. and Castelli, R. A., 2003, **Immiscibility in the Fe_3O_4-$FeCr_2O_4$ spinel binary**: *Journal of Physics & Chemistry of Solids, v.64*, no.11, p.2081-2091.
A recent thermodynamic model of mixing in spinel binaries, based on changes in cation disordering between tetrahedral and octahedral sites, gives poor agreement with measured consolute solution temperature and solvus for the Fe_3O_4-$FeCr_2O_4$ system under conditions where incomplete mixing occurs. A revised model including (1) ordering of magnetic moments of cations in the tetrahedral sublattice antiparallel to the moments of those in the octahedral sublattice and (2) pair-wise electron hopping between octahedral site Fe^{3+} and Fe^{2+} ions predicts a consolute solution temperature (T_{cs}) = 600°C and a solvus at 500°C of n = 0.05 and 0.70 for the Fe ($Fe_{1-n}Cr_n)_2O_4$ spinel binary.

Modeling and Theory

Carvallo, C., Muxworthy, A. R., Dunlop, D. J. and Williams, W., 2003, **Micromagnetic modeling of first-order reversal curve (FORC) diagrams for single-domain and pseudo-single-domain magnetite**: *Earth & Planetary Science Letters, v.213*, no.3-4, p.375-390.
A conjugate-gradient micromagnetic model yields a FORC diagram with a single peak at H_c for individual elongated SD. For a vortex PSD grain we observe multiple FORC peaks. In a 2x2x2 array of elongated SD particles, a secondary branch on the reversal curves appears if the spacing D between particles is less than about twice the particle length L. This feature translates into the appearance of one negative and three positive peaks on the FORC diagram. For a 3x3x3 array of particles, we again observe several secondary branches when D<2L, leading to the appearance of multiple peaks on the FORC diagram. Splitting of the central peak on the H_u axis when particles interact could explain the vertical spread of FORC distributions of natural interacting samples.

Davila, A. F., Fleissner, G., Winklhofer, M. and Petersen, N., 2003, **A new model for a magnetoreceptor in homing pigeons based on interacting clusters of superparamagnetic magnetite**: *Physics & Chemistry of the Earth, v.28*, no.16-19, p.647-652.
Potentially magnetoreceptive nerve cells comprise chain-like aggregates with up to 20 closely spaced clusters of SP magnetite. Experiments on SP model systems simulate the behaviour of the aggregates in varying magnetic fields. Magnetic-field induced interactions between the clusters in an aggregate gives rise to attractive and repulsive forces between the clusters. The resulting stress on the surrounding cellular structures varies with field direction and intensity.

Fabian, K., 2003, **Statistical theory of weak field thermoremanent magnetization in multidomain particle ensembles**: *Geophysical Journal International, v.155*, no.2, p.479-488.
A non-equilibrium statistical theory of MD TRM describes thermal magnetization changes as continuous inhomogeneous Markov processes. From three very general physical properties of TRM, the linearity of TRM with field is derived for generic MD particle ensembles. The general validity of Thellier's law of additivity of partial TRM's in weak fields is established and a method for proving a large class of similar additivity laws is developed. The theory allows consistent treatment of blocking and unblocking of remanence in multidomain particle ensembles and naturally explains apparent differences between blocking and unblocking temperatures.

Morup, S., 2003, **Spin-canting and transverse relaxation at surfaces and in the interior of ferrimagnetic particles**: *Journal of Magnetism & Magnetic Materials, v.266*, no.1-2, p.110-118.
Analytical expressions for the magnetic energy and the spin-canting angles in some simple ferrimagnetic bulk and surface structures are presented. It is shown that the energy barriers separating different spin-canted states often will be very small. Therefore, the spin canting may be static only at very low temperatures and dynamic at higher temperatures. The calculations elucidate the field dependence of the canting angles, the high-field susceptibility of complex magnetic materials, the high-frequency susceptibility of diamagnetically substituted ferrites, and the apparently temperature-independent relaxation phenomena at very low temperatures.

Muxworthy, A., Williams, W. and Virdee, D., 2003, **Effect of magnetostatic interactions on the hysteresis parameters of single-domain and pseudo-single-domain grains**: *Journal of Geophysical Research-Solid Earth, v.108*, no.B11, 2517.
A three-dimensional micromagnetic study shows that interactions can strongly affect the magnetic characteristics of assemblages of ideal SD grains and cubic grains between 30-250 nm in size. For example, assemblages of interacting SD grains can plot in the traditional MD area of the Day plot. For grains > 100 nm in size, interactions can have the opposite effect, and can cause the hysteresis parameters to shift toward the SD region of the Day plot. The SD/MD transition size increases as the interaction spacing is decreased.

Shcherbakov, V. P. and Sycheva, N. K., 2003, **Mathematical modeling of biased hysteresis loops in the presence of exchange anisotropy at an interface**: *Izvestiya-Physics of the Solid Earth, v.39*, no.8, p.685-692.
A rigorous theory of biased hysteresis loops in exchange-coupled ferro-antiferromagnetic bilayers shows that domain wall creation decreases the loop bias field H_{bs} by two orders of magnitude, bringing H_{bs} into agreement with observed values. The H_{bs} value is shown to reach a few hundreds of oersted for solid-state exsolution structures in bilayers of the maghemite-hematite and hemoilmenite-hemoilmenite (with different Ti concentrations) types if the ferromagnetic phase is SD. The bias can be extremely small (~1 Oe) for MD particles.

Szotek, Z., *et al.*, 2003, **Ab initio study of charge order in Fe_3O_4**: *Physical Review B, v.6805*, no.5, 4415.
We present a self-interaction corrected local spin-density study of the electronic structure and possible charge order of magnetite Fe_3O_4. The issue of charge order in magnetite is explored in both cubic and orthorhombic structures, the latter being an approximation to the true, low-temperature, monoclinic structure. We find that the Verwey charge ordered phase is not the ground-state solution for this compound either in cubic or orthorhombic structure. We conclude that the structural distortions, more than localization/delocalization correlations, are responsible for the charge disproportionation in the low-temperature phase.

Synthesis and Properties of Magnetic Materials

Fu, Y. Y., *et al.*, 2003, **Synthesis of large arrays of aligned α-Fe_2O_3 nanowires**: *Chemical Physics Letters, v.379*, no.3-4, p.373-379.
Synthesized α-Fe_2O_3 nanowire arrays are comprised of perfect single crystals with diameters of 20-40 nm and lengths of 2-5 μm. The high surface density of the nanowires (10^8-10^9 cm^{-2}) is considered to be responsible for the aligned growth. The size of the α-Fe_2O_3 nanowires may be tailored to required dimension by adjusting the flowing rate of the gases as well as the time and temperature of reaction, offering opportunities for both fundamental research and technological applications.

Itoh, H. and Sugimoto, T., 2003, **Systematic control of size, shape, structure, and magnetic properties of uniform magnetite and maghemite particles**: *Journal of Colloid & Interface Science, v.265*, no.2, p.283-295.
As an application of the gel-sol method especially developed for the synthesis of general monodisperse particles in large quantities, uniform hematite (α-Fe_2O_3), magnetite (Fe_3O_4), and maghemite (γ-Fe_2O_3) particles, precisely controlled in size, aspect ratio, and internal structure, have been prepared.

Lian, S. Y., *et al.*, 2003, **Convenient synthesis of single crystalline magnetic Fe_3O_4 nanorods**: *Solid State Communications, v.127*, no.9-10, p.605-608.
Uniform single-crystal magnetic Fe_3O_4 nanorods synthesized in a solution-phase approach have average diameters of ca. 80 nm and lengths of up to 2 μm. The composition of the nanorods is appraised by X-ray photoelectron spectroscopy (XPS). TEM images show that the magnetite particles are homogenous and have the shape of rods.

Vargas, J. M., *et al.*, 2003, **Structural, magnetic, and Mössbauer characterization of size-controlled iron-iron oxide nanoparticles obtained by chemical methods**: *IEEE Transactions on Magnetics, v.39*, no.5 Part 2, p.2681-2683.
Size-controlled Fe nanoparticles have been obtained by thermal decomposition of $Fe(CO)_5$ in organic solution. Samples with different sizes, in the 6-12 nm range, have been characterized by high-resolutibn TEM, XRD, Mössbauer spectroscopy, and magnetization measurements. All samples present narrow size distributions and superparamagnetic behavior. Exposure to air leads to the formation of a polycrystalline phase, mainly Fe_3O_4.

...VF Reports
continued from p. 3

Temperature dependence of magnetic hysteresis

Yongjae Yu
Scripps Institution of Oceanography
UC San Diego
yjyu@ucsd.edu

Knowledge of the temperature dependence of hysteresis properties is useful in deciphering dominant anisotropy and/or changes in domain states. Although the low-temperature hysteresis properties of titanomagnetites have been extensively studied, the high-temperature hysteresis properties of (titano)magnetites have been relatively less studied.

I used seven synthetic magnetite powders whose mean grain sizes range from single domain (SD; 65 nm) to small multidomain (MD; 16.9 μm). For each grain size, three sets of powders were prepared. The first set of powders is 0.5% by volume dispersions of magnetite in a matrix of CaF_2. These were vacuum-sealed in quartz capsules of 3 cm and annealed for 3 hr at 700C to stabilize the magnetic properties. The quartz capsules were unsealed just prior to hysteresis measurements. The second set of powders is 0.5% volume dispersions of unannealed magnetite in a matrix of CaF_2. The third set is bulk magnetites.

Natural samples were also studied: CG (Cordova Gabbro, ON, Canada); KM (Kometsuka basalts, Mt. Aso, Japan); MORB 1-7 (zero-age mid-oceanic ridge basalts, East Pacific Rise); sbg (submarine basaltic glass, ODP 807C}; and TG-A, TG-B (Tudor Gabbro, ON, Canada).

Hysteresis properties have been measured at a series of temperatures between 20 K and 600C in the peak field of 1 T (field increments were 10 mT). The signal averaging time was usually set to 200 ms, but 1 s was used for weak samples.

For synthetic samples and gabbros, shape anisotropy dominates most temperature ranges. However, exchange anisotropy dominates above 540-560C while magnetostrictive anisotropy controls hysteresis properties below 120 K. Titanomagnetite-bearing oceanic basalts show quite different behavior with much higher coercivity, resulting from prominent magnetostrictive anisotropy. While many factors such as composition, field-treatment, grain shape and size, and stress affect hysteresis properties at various temperature ranges, a dominant anisotropy was better recognized when remanence ratio was plotted against coercivity.

I appreciate Mike Jackson, Jim Marvin, and Peat Solheid of the Institution for Rock Magnetism (IRM) for their help with the measurements. Jeff S. Gee generously donated a large collection of MORBs for use in this study. Lisa Taxue and Bruce M. Moskowitz shared fruitful discussions.

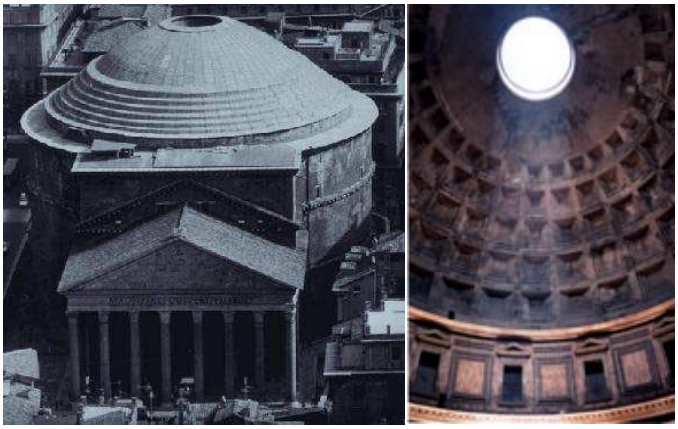

The Pantheon in Rome, with its 43-m-diameter pozzolanic concrete dome

...pozzolana

continued from p. 1

silica (SiO_2)). Crushing and "burning" (heating to ~1500° C) these produces a mixture of di-, tri- and tetra-calcium silicates, aluminates and aluminoferrites. When these are subsequently mixed with water, the hydration reaction forms a colloidal gel of calcium-aluminum silicate hydrate, with high internal surface forces that bind it together with other building materials.

The burning or calcination that renders the raw ingredients reactive occurs naturally in pozzolans. As Vitruvius puts it, "therefore the fire and vapor of flame within, flowing through the cracks, makes that earth light. And the tufa which is found to come up there is free from moisture. Therefore when three substances formed in like manner by the violence of fire come into one mixture, they suddenly take up water and cohere together. They are quickly hardened by the moisture and made solid, and can be dissolved neither by the waves nor the power of water."

The Pantheon in Rome, one of the landmarks in the history of architecture, is equally a triumph of engineering and applied materials science. Its hemispheric dome, 43 meters in diameter, has stood for nearly two millennia, and was until modern times the largest in the world. The structure is built primarily of concrete, with pozzolana both in the aggregate blocks and in the mortar binding the blocks together. The aggregate materials were assembled with a gradation in density: heavy travertine in the foundation and walls, proceeding to lighter materials such as pumice at the top, and culminating in the great open oculus. Over the centuries a series of radial cracks has developed, extending from the base of the dome upward towards the oculus, caused by the circumferential tensile stress due to the enormous weight of the dome, which consequently acts not as a single cohesive structure but as a set of radial arches interlocked by a keystone ring around the oculus.

The Colosseum is another enduring pozzolana and masonry structure, and we may also mention the aqueducts. Although the early ones (such as the Pont du Gard) were made of massive cut stone blocks, remarkably and laboriously fitted together with no mortar, the later ones (e.g., Merida) were made elegantly and economically from continuous pozzolana concrete cores, with facings of stone or brick.

Magnetic Composition of Pozzolana Cements

But let's get to the point. One of the characteristics of our pozzolana cement that makes it suitable for use as an interlab standard is that it is quite strongly magnetic. Hysteresis measurements (Fig 1a) show a saturation magnetization around 0.6 to 0.7 Am^2/kg, equivalent to a magnetite/maghemite content of nearly 1% by mass. Although portland cements nearly all contain some iron (typically 0.5-5%), it is likely that the majority of this magnetically-ordered phase originates in the pozzolanic ash in the mixture; both volcanic ash [e.g., Heider et al., 1993; Rosenbaum et al., 1993; Pawse et al., 1998; Evans, 1999] and industrial fly ash [e.g., Dekkers & Pietersen, 1992; Gomes et al., 1999; Hanesch & Petersen, 1999; Hower et al., 1999] often contain abundant fine-particle ferrimagnets. In our pozzolana cement samples, a dominantly single-domain and pseudo-single-domain state is indicated by the M_R/M_S ratio of about 0.3.

The ferrimagnetic phase in these pozzolana cements appears to be dominantly oxidized magnetite or maghemite, as shown by the Curie temperature exceeding 600° C (Fig 1b), and by the absence of any low-temperature transitions (Fig 3, 4). Although maghemite is unstable and inverts to hematite at high temperatures, fine-grained maghemites survive to temperatures exceeding 700° C [Özdemir and Banerjee, 1984; Özdemir, 1990; de Boer and Dekkers, 1996]. Mössbauer spectroscopy of bulk pozzolana cement powder shows sextets of both Fe^{2+} and Fe^{3+} in magnetically-ordered phases, in a proportion roughly halfway between those of stoichiometric magnetite and maghemite (Fig 2).

The low-temperature remanence characteristics (Fig 3a) strongly resemble those of oxidized synthetic fine-grained (~50 nm) magnetite (e.g. the Wright 4000 sample in the Rock Magnetic Bestiary <*www.geo.umn.edu/orgs/irm/bestiary/index.html*>). The remanence that results from cooling (300-20 K) in a 2.5 T field is slightly larger than a low-temperature (20 K) 2.5-T isothermal remanence, and the difference between the two gradually diminishes on warming. This qualitatively resembles the behavior of goethite, and is probably due to the same phenomena: incomplete saturation in 2.5 T at 20 K, and more efficient magnetization by cooling in a strong field. This FC-ZFC behavior is distinctly different from that of stoichiometric magnetite, where the differences in intensity (attributable to anisotropy induced by field-cooling) disappear abruptly on warming through the Verwey transition at T_V~120 K.

The room-temperature hysteresis loop in a maximum field of 1 T (Fig 1a) shows a small curvature even near the peak field, indicating not-quite-complete saturation. Measurements in higher fields, up to 2.5 T, show that indeed the high-field slope continues to decrease slightly, even above 2 T. Thus a small amount of hard antiferromagnetic material is also present. The temperature dependence of the high-field susceptibility (Fig 3b) shows that it is dominantly paramagnetic in origin, and the values indicate that the paramagnetic iron content is <1% by mass. M_S and M_R are nearly independent of temperature below 300 K.

Magnetic Kinetics: Frequency- and Rate-Dependent Behavior

In contrast to the brute simplicty of strong-field measurements, interlab calibration of weak-field remanence properties is made more interesting/difficult by the sensitivity of the magnetization process to a variety of factors. For example, there is a surprisingly strong dependence of both pTRM and pARM intensities on prior "conditioning" of the sample [e.g.,

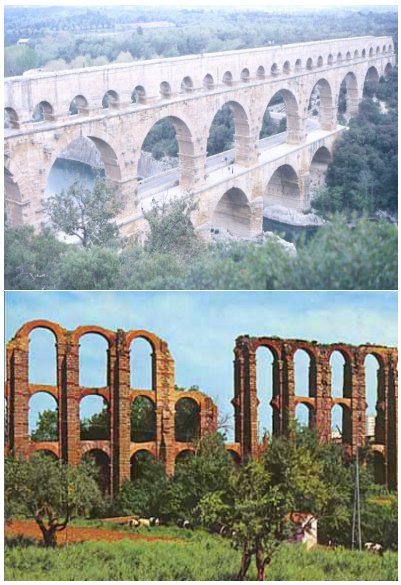

Top: the Pont du Gard, built ca 19 BCE, using massive cut stones and no mortar. Maximum height is 47 m .
Bottom: Los Milagros aqueduct (late 1st Century), near Merida Spain. Concrete with stone facing; height 25 meters.

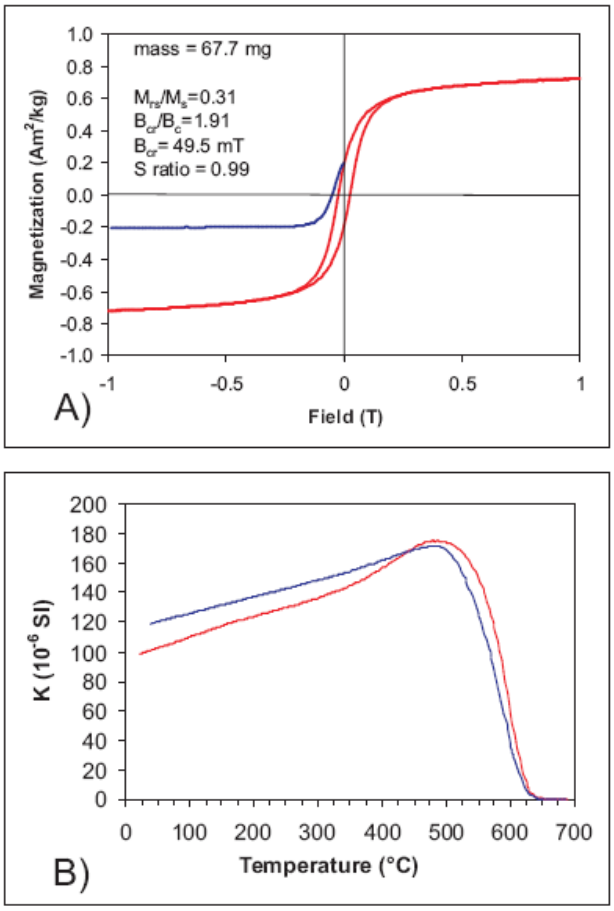

Fig 1. (a) high-field hysteresis and back-field remanence measurements show a fairly high concentration of fine-grained ferrimagnetic material. (b) Thermomagnetic beyhavior is quasi-reversible, showing a single dominant phase with a Curie temperature near 640° C.

Halgedahl, 1993; Shcherbakov et al., 2001; Yu et al., 2002]. Some of the most interesting and diagnostic magnetic behavioral characteristics are related to time-dependence. These are also less reproducible between laboratories than static bulk properties are, in large part because frequency-, rate- and time-dependence are second-order properties, that is, they are based on differences that are relatively small in proportion to the "mean" value of a property.

Our pozzolana cement samples contain a large proportion of SD grains, as well as significant fractions of SP and PSD material. There is a frequency-dependence of susceptibility that amounts to approximately 3% per decade, at room temperature and all the way down to about 40 K (Fig 4). The quasi-linear increase in susceptibility with temperature from ~50K to ~700K is consistent with a broad lognormal size distribution of SP-SD grains [Worm, 1998].

In the interlaboratory cross-calibration study, a major cause of the large variability in measured anhysteretic susceptibilities was the AF decay rate (Fig 5). Measurements with systematically-varying decay rates show a drop of approximately 4% per decade up to about 10 µT/half-cycle (using Schoenstedt and DTech instruments), and a much more rapid decrease - nearly 30% per decade - at higher decay rates (using a 2G in-line system). It is interesting that the change in slope occurs where the AF decrement per half cycle becomes comparable to the DC

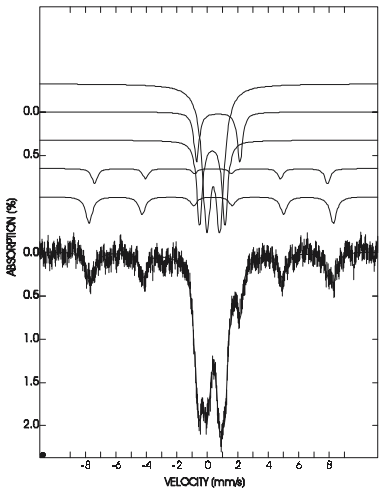

Fig 2. Mössbauer spectrum (room-temperature, zero-field) for bulk uncured pozzolana cement, and fit components including (from top) 3 paramagnetic doublets, and 2 magnetically-ordered sextets for magnetite's B [$Fe^{2.5+}$] and A [Fe^{3+}] sites. The ferrous/ferric ratio (≤1) is roughly halfway between that of stoichiometric magnetite and maghemite.

bias field. On the other hand, high-decay-rate ARMs from other instruments in different labs have much higher intensities, more in line with those produced by our Schoenstedt and DTech instruments. Another major cause of variability therefore appears to be the mode of AF decay: in the in-line system the AF maintains a constant amplitude, and a sample experiences a decaying AC field as it is transported out and away from the coil; in the other instruments the sample is stationary and the field decays. Note that the decay rate for the in-line

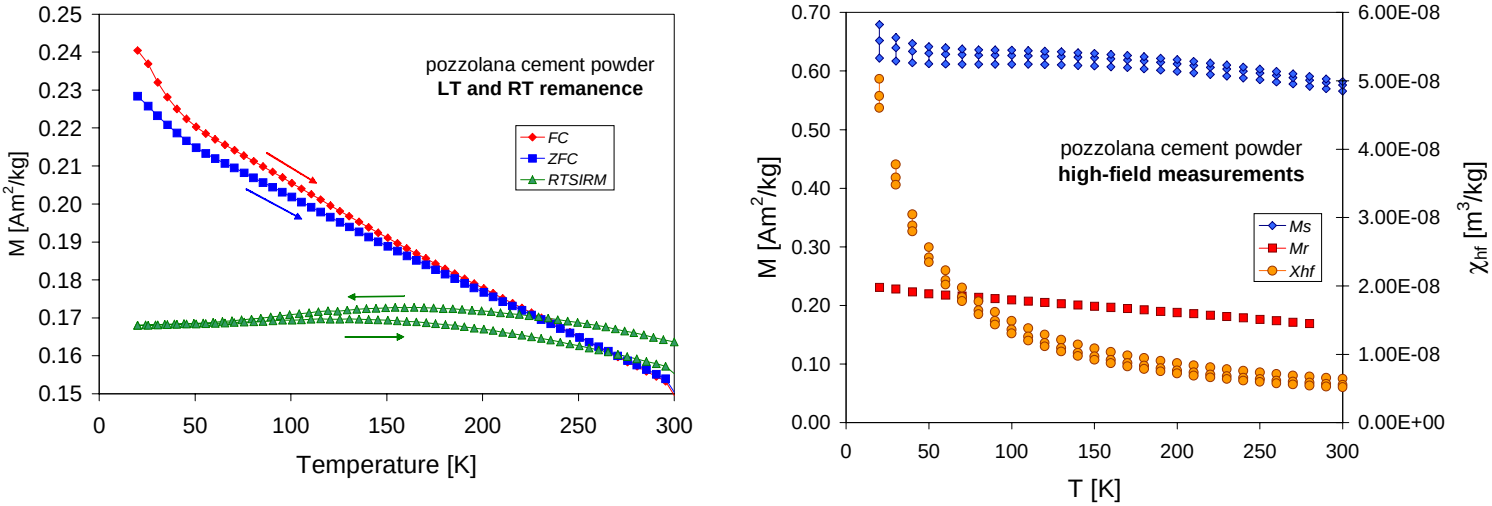

Fig 3. (a, left) Low-temperature cycling of room-temperature SIRM (RTSIRM, circles), and zero-field warming curves for remanences acquired by field-cooling (FC, diamonds, cooled in 2.5 T) and isothermally in 2.5 T at 20 K after zero-field cooling (ZFC, squares). (b, right) Parameters of low-temperature hysteresis loops, measured to maximum fields of 2.5 T: saturation remanence (M_r, squares); high-field slope (χ_{hf}, circles) and saturation magnetization (M_s, diamonds) were calculated at each temperature for field intervals 1-1.5 T, 1.5-2T, and 2-2.5T; inequality of the three values shows degree of non-linearity, due to incomplete ferromagnetic saturation and/or partial paramagnetic saturation at the lowest temperatures.

continued on p. 10...

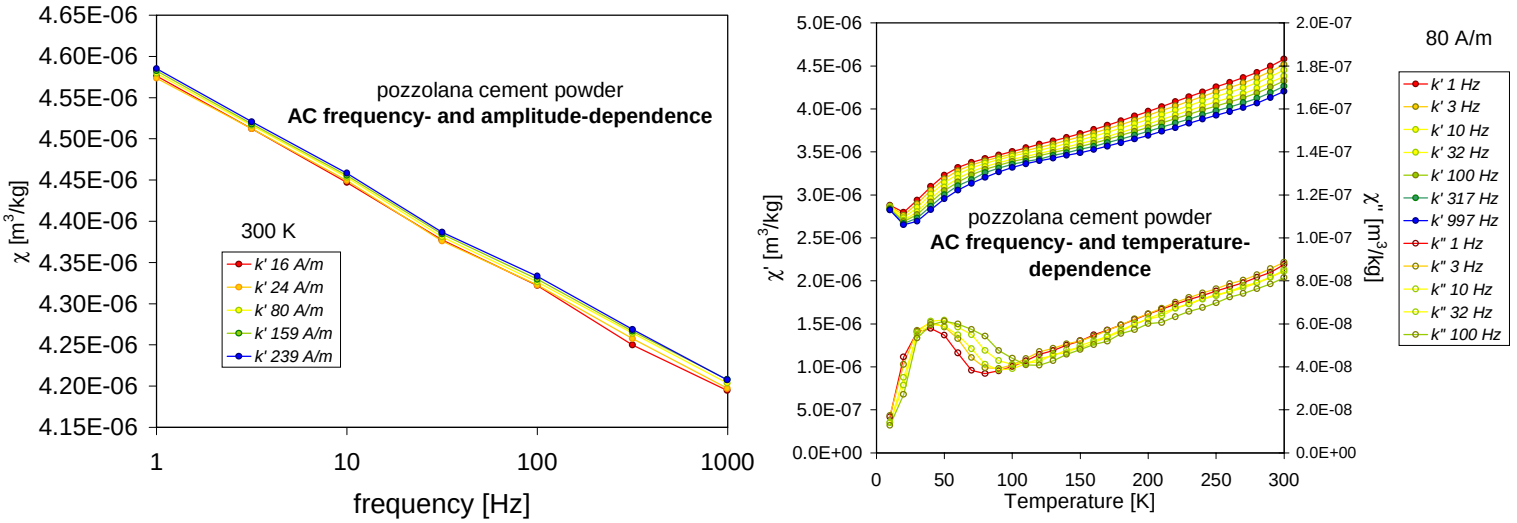

Fig 4. (a, left) Room-temperature frequency- and amplitude-dependence of ac susceptibility; the former is ~2.8% per decade, and the latter is insignificant. (b, right) Temperature- and frequency-dependence (H_{ac}=80 A/m). Paramagnetic susceptibility becomes significant only at the lowest temperatures. The strong frequency dependence above 30 K, and the quasi-linear increase in susceptibility with temperature, indicate a relatively broad distribution of SP grainsizes.

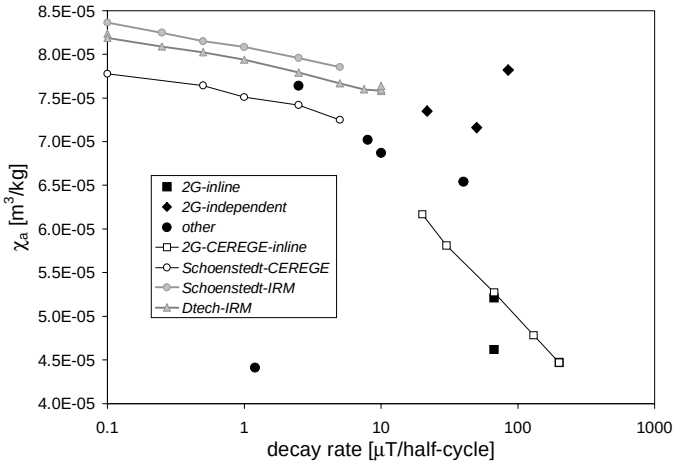

Fig 5. Anhysteretic susceptibilities (100 mT AC, 50 μT DC) determined for a set of pozzolana cement samples in the MAG-NET interlab calibration study (solid symbols) and in subsequent measurements at CEREGE (open symbols, black lines) and at IRM (gray). There is a trend of decreasing χ_A with increasing AF decay rate; for the magnetizers at IRM the average drop is about 4% per decade. In-line magnetizers, where the decay rate is governed by field geometry and translation speed, produce systematically lower ARMs. The differences between the IRM and CEREGE Schoenstedt results may be due in part to the use of different specimens, and in part to the use of mu-metal shielding and DC coils at IRM, whereas the CEREGE ARMs were imparted in the terrestrial field.

...pozzolana

continued from p. 9

systems is therefore not constant, but changes with time, position and amplitude; the in-line decay rates in Fig 5 are averages, calculated by the method of Brachfeld [1999].

Dunlop and Yu [2003] have observed experimentally that ARM intensities diminish with increasing decay rate for SD and PSD assemblages, but increase for MD grains, mimicking the dependence of TRM on cooling rate and grain size. The decrease is attributed to less complete equilibration with the bias field at higher decay rates; thermal activation theories of Néel [1949] and Egli & Lowrie [2002] predict decreases of 6-11% per decade for SD assemblages. For this reason, one might also expect a similar dependence of χ_a on AF frequency. The Schoenstedt instrument at IRM operates at 397 Hz, and the DTech at 137 Hz, nearly 3 times slower. For a decay rate of 0.1 μT/half-cycle, each instrument completes 500,000 cycles during the decay from a peak of 100 mT, but the DTech takes a leisurely 61 minutes to complete the process, whereas the Schoenstedt speeds through in 21 minutes. Ergo, kinetics should yield somewhat higher ARMs from the DTech, for the same AC and DC fields. Interestingly, however, we find just the opposite, despite careful calibration of AC and DC fields.

Which brings us back to the idea of preconditioning. Because of differences in ARM circuitry, the Schoenstedt and DTech instruments handle the DC field differently: in the former the DC field is on during both the ramping up and ramping down of the AC field; in the latter the DC field is only switched on after the peak AC amplitude has been reached, remaining on during the decay. It seems that the additional application of the DC field during ramp-up in the Schoenstedt may outweigh the kinetic disadvantage of its higher frequency. However this is not easy to test, since it requires changing the way the instruments work.

Further Interlab Comparisons and Calibrations

Previous interlaboratory calibration studies [Snowball et al., 1994; Sagnotti et al., 2003] have been conducted as blind tests, with "expected" values unknown to the participants. Here we propose a more open approach for follow-up studies. Detailed experimental data for these samples are available in Sagnotti et al. [2003] and in this article. On request, we will send you a solid 2x2x2-cm cube of pozzolana cement, and/or a small vial of uncured powder suitable for measurement in various instruments. You can use these to compare the behavior of your magnetizing and measurement instruments to those of the previously-tested labs. We are particularly interested in further work illuminating the intricate dependence of anhysteretic susceptibility on details of the magnetizing process, and would like to see measurements made using a wide variety of approaches and instruments.

If you would like to receive a pozzolana cement specimen, send your request to the IRM (irm@umn.edu). In order to maximize distribution efficiency, we would like to receive requests no later than March 1, 2004, after which we will begin sending the specimens. Please indicate whether you need a solid cube or powder.

The same material that holds together the ancient structures of the Eternal City can also help tie together the worldwide set of laboratories working on rock- and mineral magnetism, and help ensure greater consistency of data, procedures and analyses.

References and Information Sources

Brachfeld, S., 1999, Separation of geomagnetic paleointensity and paleoclimate signals in sediments: examples from North America and Antarctica, Thesis (Ph. D.), University of Minnesota.

de Boer, C. B., and Dekkers, M. J., 1996, Grain-size dependence of the rock magnetic properties for a natural maghemite: *Geophysical Research Letters, v. 23*, no. 20, p. 2815-2818.

Dekkers, M. J., and Pietersen, H. S., 1992, Magnetic properties of low-Ca fly ash: a

Volta, Alessandro

b. Feb 18, 1745, Como, Lombardy [Italy]
d. March 5, 1827, Como

Alessandro Giuseppe Antonio Anastasio Volta is remembered for his 1775 development of the electrophorus, a device for generating static electricity, and especially for invention by 1800 of the "voltaic pile," the first electric battery. Following the discovery by his friend Luigi Galvani of the effects of dissimilar metals in contact with animal nerve tissue, it was controversial whether the fundamental phenomenon involved inherent animal electricity or metallic origins. In honor of Volta's demonstration that electricity could be generated inorganically, the unit of electrical potential was named for him in 1881. Volta was also the discoverer of methane gas, which he isolated in 1778.

rapid tool for Fe-assessment and a survey for potentially hazardous elements: *Materials Research Society Symposium Proceedings, v. 245*, p. 37–47.

Dunlop, D J, and Y. Yu, 2003, The dependence of anhysteretic remanent magnetization on alternating field decay rate: Fundamental origin and paleomagnetic applications: *Eos Trans. AGU, 84(46), Fall Meet. Suppl.*, Abstract GP31A-06, 2003

Egli, R., and Lowrie, W., 2002, Anhysteretic remanent magnetization of fine magnetic particles: *Journal of Geophysical Research-Solid Earth, v. 108*, no. B2, p. art. no. 2209.

Evans, M. E., 1999, Magnetoclimatology: a test of the wind-vigour model using the 1980 Mount St. Helens ash: *Earth and Planetary Science Letters, v. 172*, no. 3, p. 255-9.

Gomes, S., et al., 1999, Characterization of magnetite in silico-aluminous fly ash by SEM, TEM, XRD, magnetic susceptibility, and Mössbauer spectroscopy: *Cement and Concrete Research, v. 29*, p. 1705-1711.

Hanesch, M., and Petersen, N., 1999, Magnetic properties of a recent parabrown-earth from Southern Germany: *Earth and Planetary Science Letters, v. 169*, no. 1-2, p. 85-97.

Heider, F., Körner, U., and Bitschene, P., 1993, Volcanic ash particles as carriers of remanent magnetization in deep-sea sediments from the Kerguelen Plateau: *Earth and Planetary Science Letters, v. 118*, p. 121-134.

Halgedahl, S. L., 1993, Experiments to investigate the origin of anomalously elevated unblocking temperatures: *Journal of Geophysical Research B: Solid Earth, v. 98*, p. 22,443–22,460.

Hower, J. C., et al., 1999, Petrology, mineralogy, and chemsitry of magnetically-separated fly ash: *Fuel, v. 78*, p. 197-203.

Néel, L., 1949, Théorie du traînage magnétique des ferromagnétiques en grains fins avec applications aux terres cuites: *Annales de Géophysique, v. 5*, p. 99–136.

Özdemir, Ö. 1990, High-temperature hysteresis and thermoremanence of single-domain maghemite: *Physics of the Earth and Planetary Interiors, v. 65*, p. 125–136.

Özdemir, Ö., and Banerjee, S. K., 1984, High temperature stability of maghemite (γ-Fe_2O_3): *Geophysical Research Letters, v. 11*, p. 161–164.

Pawse, A., Beske-Diehl, S., and Marshall, S. A., 1998, Use of magnetic hysteresis properties and electron spin resonance spectroscopy for the identification of volcanic ash: a preliminary study: *Geophysical Journal International, v. 132*, p. 712-720.

Rosenbaum, J. G., 1993, Magnetic grain-size variations through an ash-flow sheet: influence on magnetic properties and implications for cooling history: *Journal of Geophysical Research B: Solid Earth, v. 98*, p. 11,715–11,727.

Sagnotti, L., Rochette, P., Jackson, M., Vadeboin, F., Dinares-Turell, J., and Winkler, A., 2003, Inter-laboratory calibration of low-field magnetic and anhysteretic susceptibility measurements: *Physics of the Earth & Planetary Interiors, v. 138*, no. 1, p. 25-38.

Shcherbakov, V. P., Shcherbakova, V. V., Vinogradov, Y., and Heider, F., 2001, Thermal stability of pTRMs created from different magnetic states: *Physics of the Earth and Planetary Interiors, v. 126*, no. 1, p. 59-73.

Snowball, I., C. Hunt, and B. Moskowitz, 1994, Initial inter-laboratory calibration effort: A lesson in trial and error?: *IRM Quarterly, v. 4*, n. 1.

Worm, H.-U., 1998, On the superparamagnetic-stable single domain transition for magnetite, and frequency dependence of susceptibility: *Geophysical Journal International, v. 133*, p. 201-206.

Yu, Y., Dunlop, D. J., and Ozdemir, O., 2002, Partial anhysteretic remanent magnetization in magnetite. 2. Reciprocity: Journal of Geophysical Research, v. 107, no. B10, 2245, doi:10.1029/2001JB001269.

http://www.geo.uu.nl/~magnet/MAGazine/Magazine.htm

http://www.globalcolleges.com/spain/aqueduct-merida.jpg

http://www.chass.utoronto.ca/~wulfric/varia/photos-fr/pont-du-gard1.jpg

http://www.unf.edu/classes/freshmancore/core1images/pantheon.jpg

http://kevino.net/images/kevino.net/p-rome-pantheon--2.jpg

New and Recent Visiting Fellows

2003B

Sue Beske-Diehl, *Michigan Tech University*, Environmental signal in rock magnetic properties of Lake Superior sediments.

Claire Carvallo, *University of Toronto at Mississauga*, Characterization of N-type titanomaghemite in submarine basalt from Koko seamount, and FORC diagrams of submarine basalts and elongated SD natural samples.

Yongxiang Li, *Lehigh University*, Do magnetic properties of sediments from White Lake, northwestern New Jersey, indicate climate changes?

Stephanie Maes, *University of Wisconsin-Madison*, Separating complex anisotropies with high-field AMS: Insizwa complex, South Africa.

Robert Musgrave, *Monash University*, Rock-magnetic signature of the bacterial response to gas hydrate: implications for palaeoceanography and palaeoclimate.

Donald Thieme, *University of Georgia*, Environmental magnetism of Susquehanna Valley alluvium.

David Williamson, *CEREGE*, Magnetic enhancement in volcanic ash soils from the tropics: glass dissolution, authigenesis of (ultra)fine iron oxides, or wet deposition?

Yongjae Yu, *Scripps Institution of Oceanography*, Magnetic properties of chromite.

2004A

Milagrosa Aldana, *Universidad Simón Bolívar*, Identification of magnetic authigenesis in drill-cuttings from Venezuelan oil fields.

Laurent Carporzen, *Institut de Physique du Globe de Paris (IPGP)*, Superparamagnetic magnetite contribution to the magnetic properties of shocked rocks from the Vredefort Meteorite Crater.

Vincent Chevrier, *CEREGE*, Weathering of iron rich phases in a Martian atmosphere.

Jennifer Inwood, *University of Plymouth*, Rock magnetic characterization of the carriers of stable, pre-deformational magnetizations in a Tethyan ophiolite (Hatay, Turkey).

Adrian Muxworthy, *University of Edinburgh*, Understanding MD remanence: Viscous magnetization of MD magnetite and Assessing magnetostatic interactions between different mineral phases.

Anne-Lise Salomé, *Institut de Physique du Globe de Paris (IPGP)*, Characterization of magnetic mineralogy for sands/rocks from La Martinique Island and for lacustrines sediments from Lebanon.

Xixi Zhao, *University of California Santa Cruz*, Rock magnetic investigation of serpentinized peridotite from the Newfoundland Margin, ODP Leg 210.

The *Institute for Rock Magnetism* is dedicated to providing state-of-the-art facilities and technical expertise free of charge to any interested researcher who applies and is accepted as a Visiting Fellow. Short proposals are accepted semi-annually in spring and fall for work to be done in a 10-day period during the following half year. Shorter, less formal visits are arranged on an individual basis through the Facilities Manager.

The *IRM* staff consists of **Subir Banerjee**, Professor/Director; **Bruce Moskowitz**, Professor/Associate Director; **Jim Marvin**, Senior Scientist; **Mike Jackson**, Senior Scientist and Facility Manager, and **Peat Sølheid**, Scientist.

Funding for the *IRM* is provided by the **National Science Foundation**, the **W. M. Keck Foundation**, and the **University of Minnesota**.

The *IRM Quarterly* is published four times a year by the staff of the *IRM*. If you or someone you know would like to be on our mailing list, if you have something you would like to contribute (*e.g.*, titles plus abstracts of papers in press), or if you have any suggestions to improve the newsletter, please notify the editor:

Mike Jackson
Institute for Rock Magnetism
University of Minnesota
291 Shepherd Laboratories
100 Union Street S. E.
Minneapolis, MN 55455-0128
phone: (612) 624-5274
fax: (612) 625-7502
e-mail: irm@umn.edu
www.geo.umn.edu/orgs/irm/irm.html

IRM

UNIVERSITY OF MINNESOTA

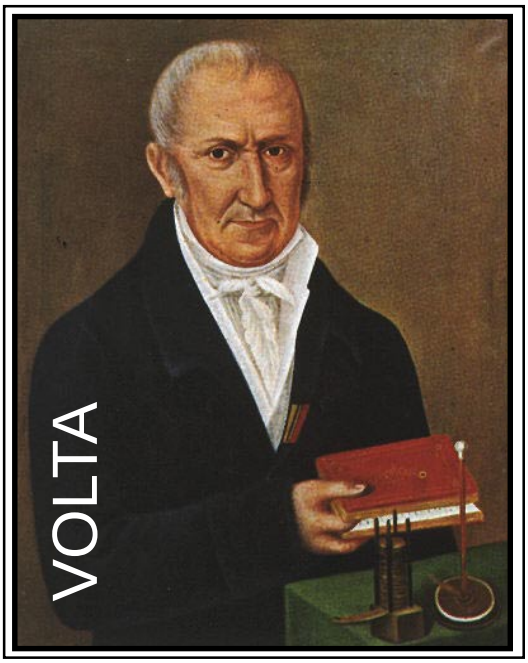

http://www.th.physik.uni-frankfurt.de/~jr/gif/phys/volta.jpg

Collector's Series #25

In the "Park of acqueducts" in Roma, where there are preserved some of the highest and longest ancient acqueducts, the most spectacular is this one, built under Caligola and Claudius (38-52 AD). (photo by Leonardo Sagnotti).

The IRM Quarterly

University of Minnesota
291 Shepherd Laboratories
100 Union Street S. E.
Minneapolis, MN 55455-0128
phone: (612) 624-5274
fax: (612) 625-7502
e-mail: irm@umn.edu
www.geo.umn.edu/orgs/irm/irm.html

Nonprofit Org.
U.S Postage
PAID
Mpls., MN
Permit No. 155